Tunable Magnon-Magnon Coupling Mediated by Dynamic Dipolar Interaction in Synthetic Antiferromagnets

Yoichi Shiota,[1,*] Tomohiro Taniguchi,[2,†] Mio Ishibashi,[1] Takahiro Moriyama,[1] and Teruo Ono[1,3]
[1]Institute for Chemical Research, Kyoto University, Uji, Kyoto 611-0011, Japan
[2]National Institute of Advanced Industrial Science and Technology (AIST), Spintronic Research Center, Tsukuba, Ibaraki 305-8568, Japan
[3]Center for Spintronics Research Network, Graduate School of Engineering Science, Osaka University, Toyonaka, Osaka 560-8531, Japan

(Received 18 February 2020; accepted 3 June 2020; published 1 July 2020)

We report an experimental observation of magnon-magnon coupling in interlayer exchange coupled synthetic antiferromagnets of FeCoB/Ru/FeCoB layers. An anticrossing gap of spin-wave resonance between acoustic and optic modes appears when the external magnetic field points to the direction tilted from the spin-wave propagation. The magnitude of the gap (i.e., coupling strength) can be controlled by changing the direction of the in-plane magnetic field and also enhanced by increasing the wave number of excited spin waves. We find that the coupling strength under the specified conditions is larger than the dissipation rates of both the resonance modes, indicating that a strong coupling regime is satisfied. A theoretical analysis based on the Landau-Lifshitz equation shows quantitative agreement with the experiments and indicates that the anticrossing gap appears when the exchange symmetry of two magnetizations is broken by the spin-wave excitation.

DOI: 10.1103/PhysRevLett.125.017203

Hybrid quantum systems based on collective spin excitations in ferromagnetic materials, called magnons, have been intensively studied in the last decade [1–14]. This is because these systems offer a promising platform for novel quantum information technologies. Understanding and exploiting the interaction in hybrid quantum systems are the key to building a large-scale artificial many-body quantum system [11–14]. These findings could lead to magnon-based functional devices [15–18] and applications of quantum technologies such as quantum computing [19,20], quantum communication [21,22], and quantum sensing [23]. In contrast to the coupling of magnons with a distinct physical quantum system (e.g., microwave and optical photon, phonon, etc.), it has recently been reported that a strong magnon-magnon coupling can be realized in several kinds of systems, which is analogous to the hybrid quantum system. The magnon-magnon coupling between the exchange spin wave in a yttrium iron garnet thin film and the ferromagnetic resonance in a ferromagnetic metal has been observed due to the interlayer exchange interaction [24–27]. Recently, coupling of antiferromagnetic magnon modes was demonstrated using a layered antiferromagnet $CrCl_3$ by MacNeill *et al.* [28] and a compensated ferrimagnet gadolinium iron garnet by Liensberger *et al.* [29]. However, because these experiments focused on magnons with uniform precession ($k = 0.0\ \mu m^{-1}$, where k is the wave number), external magnetic field tilted toward the out-of-plane direction [28] or the induction of a magnetocrystalline anisotropy [29] is necessary for systems with symmetry breaking.

In this Letter, we demonstrate the strong magnon-magnon coupling between acoustic and optic modes with an in-plane magnetic field by utilizing magnons with nonuniform precession ($k \neq 0.0\ \mu m^{-1}$) in ferromagnetic-metal-based synthetic antiferromagnets (SAFs) of FeCoB/Ru/FeCoB. The coupling strength can be tuned by the wave number k and angle φ_k between an external magnetic field and the spin-wave propagation direction. An anticrossing gap of two modes appears when the spin wave propagates in the direction of $\varphi_k \neq 0°$ and is maximized at approximately $\varphi_k = 45°$. A theoretical analysis shows quantitative agreements with the experimental results and indicates that the appearance of the anticrossing gap accompanies symmetry breaking with respect to the exchange of magnetizations.

Films of $Ta(3)/Ru(3)/Fe_{60}Co_{20}B_{20}(15)/Ru(0.6)/Fe_{60}Co_{20}B_{20}(15)/Ru(3)$ (the numbers in parenthesis are thicknesses in the unit of nanometers) were deposited using dc magnetron sputtering on thermally oxidized Si substrates. The Ru thickness was optimized to obtain antiferromagnetic coupling between two FeCoB layers [30]. The films were patterned into a circular shape with a diameter of 15 μm for uniform precession [ferromagnetic resonance (FMR)] and into a rectangular shape with $50 \times 100\ \mu m^2$ for nonuniform precession [spin-wave resonance (SWR)], and 50-nm-thick SiO_2 was then deposited for electrical isolation. Subsequently, we fabricated the antennas to create a dynamic Oersted field with single strip line coplanar waveguides for FMR and ground-signal-ground coplanar waveguides for SWR, as shown in

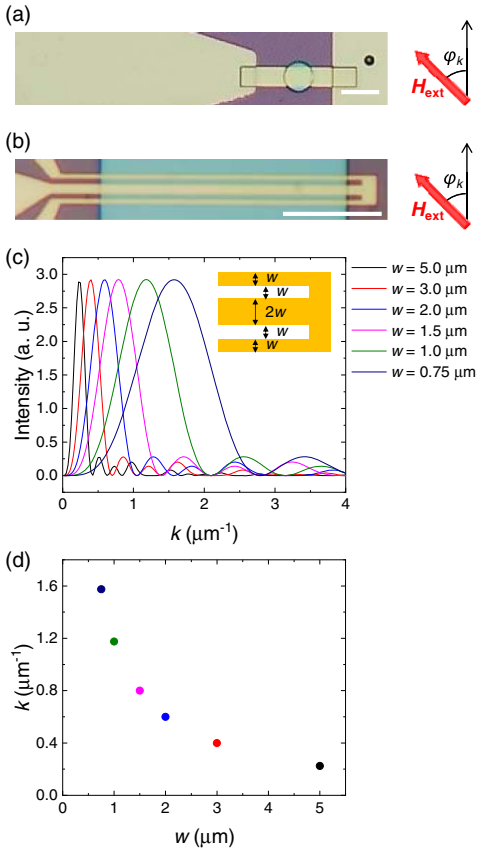

FIG. 1. Optical micrograph of the devices for investigation of (a) FMR spectra ($k = 0\ \mu\text{m}^{-1}$) and (b) SWR spectra ($k \neq 0\ \mu\text{m}^{-1}$) (scale bars: 20 μm). The external in-plane magnetic field was applied with the rotation angle φ_k, where the field magnitude varies from 0 to 150 mT with an incremental step of 2 mT. (c) The square of the Fourier spectrum of the dynamic in-plane magnetic field distribution generated by the ground-signal-ground coplanar waveguides with different widths. (d) k as a function of w, where k was determined from the peaks in (c).

Figs. 1(a) and 1(b). Excited spin waves with well-defined k were determined from the design of antennas [31]. Figure 1(c) shows the square of Fourier spectrum of dynamic in-plane magnetic field distribution generated by ground-signal-ground coplanar waveguides with different widths. The peaks correspond to the wave number of effectively excited spin waves, and this allows for the spin-wave excitation with different k, as shown in Fig. 1(d). The scattering parameter S_{11}, which is the microwave reflection occurring mainly from the antenna, was measured using a vector network analyzer to investigate the magnetic resonance. An external magnetic field was applied in the in-plane direction and rotated in the film plane with a rotation angle φ_k, as shown in Figs. 1(a) and 1(b). To extract the signal originating from the magnetic contribution, the S_{11} signals were analyzed by subtracting a reference signal obtained at a higher magnetic field. All the measurements were performed at room temperature.

Before introducing the experimental results, we describe the features of antiferromagnetic resonance modes in SAFs. It is known that SAFs exhibit two kinds of resonance precession modes in the case of the canted magnetization state: acoustic and optic modes [32,33]. At low magnetic fields ($\varphi_0 > 45°$, where φ_0 is the relative angle between the magnetization and the external magnetic field), the resonance mode of lower (higher) frequency is characterized by an in-phase (out-of-phase) precession, which is classified as the acoustic (optic) mode. At high magnetic field ($\varphi_0 < 45°$), an exchange between two modes occurs, because the resonant frequency of the acoustic (optic) mode increases (decreases) as the magnetic field increases.

Figures 2(a)–2(c) show the contour plot of the FMR spectra ($k = 0.0\ \mu\text{m}^{-1}$) at $\varphi_k = 0°$, 45°, and 90°, respectively. The two-dimensional plots are generated from the individual $\text{Re}[S_{11}]$ spectra acquired at a given applied magnetic field. When $\varphi_k = 0°(90°)$, the optic (acoustic) mode [32,33] can be effectively observed in the canted magnetization state, because each mode is coupled to the in-plane microwave field depending on the angle of a static magnetic field [28,30,34]. When the external magnetic field is applied at an intermediate angle $\varphi_k = 45°$, both the acoustic and optic modes can be observed, as shown in Fig. 2(b).

The SWR spectra ($k = 1.2\ \mu\text{m}^{-1}$) at $\varphi_k = 0°$, 45°, and 90° are shown in Figs. 2(d)–2(f), respectively. The linewidth of the SWR spectra originates from not only the intrinsic contribution but also the extrinsic contribution of the spin-wave dispersion, which is proportional to $V_g \Delta k$, where V_g is the spin-wave group velocity and Δk is the linewidth of the wave number distribution of the microwave field [31] [see Fig. 1(c)]. It should be noted that the resonance peaks of acoustic and optic modes exhibit a pronounced anticrossing gap for the SWR spectra at $\varphi_k = 45°$, while this is not the case for the FMR spectra at $\varphi_k = 45°$. In Figs. 2(g) and 2(h), we plot $(f_+ - f_-)/2$ as a function of the magnetic field for FMR and SWR spectra at $\varphi_k = 45°$, respectively, where $f_{+(-)}$ is the resonance peak of upper (lower) frequency. The minimum of $(f_+ - f_-)/2$ indicates the mutual coupling strength $g/(2\pi)$. We found that $g/(2\pi) = 0.10$ MHz for $k = 0.0\ \mu\text{m}^{-1}$ and $g/(2\pi) = 670$ MHz for $k = 1.2\ \mu\text{m}^{-1}$. Therefore, a larger k is one of the keys to increase the coupling strength between two modes.

Figure 2(i) shows the φ_k dependence of $g/(2\pi)$ for $k = 1.2\ \mu\text{m}^{-1}$. We found that the coupling strength can be tuned by rotating the in-plane magnetic field and it exhibits the maximum value at approximately $\varphi_k = 45°$. Because the spin-wave propagation direction (the vector of wave number) was defined by the antenna geometry, the rotation of the in-plane magnetic field results in a change of the relationship between the magnetization configuration and spin-wave propagation direction, as shown in the insets of Figs. 2(d)–2(f).

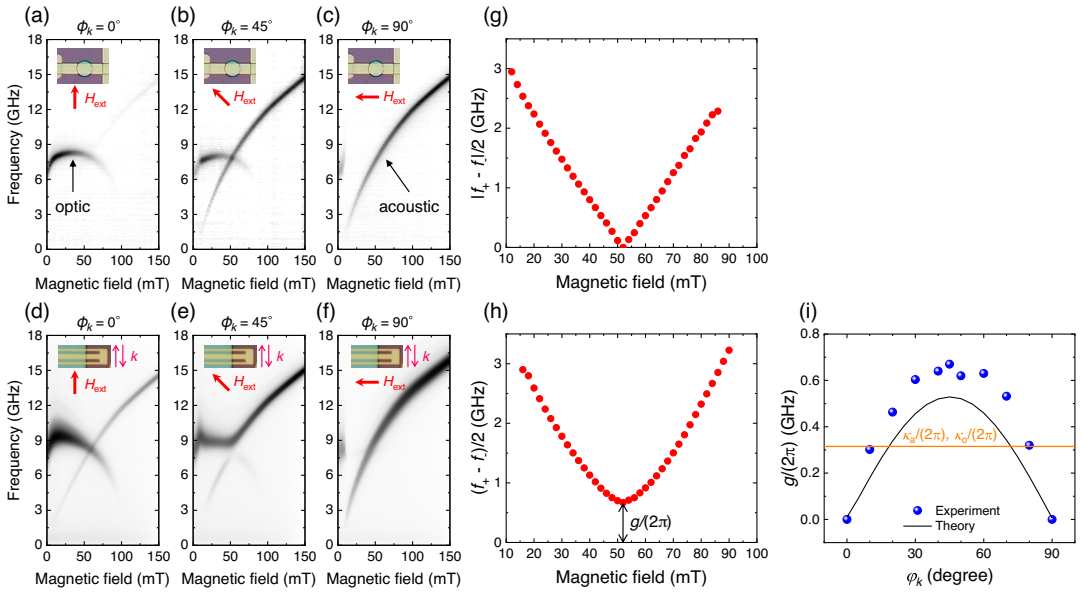

FIG. 2. Contour plots of $\mathrm{Re}[S_{11}]$ for FMR spectra ($k = 0\ \mu\mathrm{m}^{-1}$) at (a) $\varphi_k = 0°$, (b) 45°, and (c) 90°, and for SWR spectra ($k = 1.2\ \mu\mathrm{m}^{-1}$) at (d) 0°, (e) 45°, and (f) 90°. (Insets) Configuration between the device and the external magnetic field. (g),(h) $(f_+ - f_-)/2$ as a function of external magnetic field at $\varphi_k = 45°$ for FMR and SWR spectra, respectively. The minimum of $(f_+ - f_-)/2$ indicates the coupling strength $g/(2\pi)$. (i) $g/(2\pi)$ as a function of φ_k. The orange solid line indicates the dissipation rates of both the resonance modes κ_a and κ_o, determined from the half width of half maximum linewidth in the FMR spectra.

We further investigated the evolution of magnon-magnon coupling at $\varphi_k = 45°$ as a function of k by changing the widths of the coplanar waveguide. Figures 3(a)–3(e) show the contour plot of the $\mathrm{Re}[S_{11}]$ spectra with k of 0.0, 0.4, 0.8, 1.2, and 1.6 $\mu\mathrm{m}^{-1}$, respectively. As shown in Fig. 3(f), the anticrossing gap between two modes, i.e., the coupling strength, increased monotonically with increasing k. This tendency can be understood from the dynamic dipolar interaction, because the amplitude of the dipolar fields generated by the magnetization motion of spin waves is proportional to k within $|kt| < 1$ limit, where t is the thickness of ferromagnetic layer. Therefore, the magnon-magnon coupling observed in this study was mediated by the dynamic dipolar interaction between the two ferromagnetic layers in SAFs.

The dissipation rates for both the resonance modes κ_a and κ_o were determined from the half width at half maximum linewidth using FMR spectra, because the linewidth in the SWR spectra includes extrinsic broadening, as discussed above. $\kappa_a/(2\pi)$ and $\kappa_o/(2\pi)$ at the crossing point of the two modes are represented by orange solid lines in Figs. 2(i) and 3(f). The condition for a strong coupling $g > \kappa_a,\ \kappa_o$ is clearly satisfied under specified conditions, which indicates that magnon-magnon coupling with a strong coupling regime is achieved in this study.

We now present an analysis based on the Landau-Lifshitz (LL) equation to clarify the relationship between the magnon-magnon coupling in the SAFs from a theoretical viewpoint (see Supplemental Material for details [35]). A system, including two identical ferromagnetic layers FM1 and FM2 is considered. Two ferromagnets are

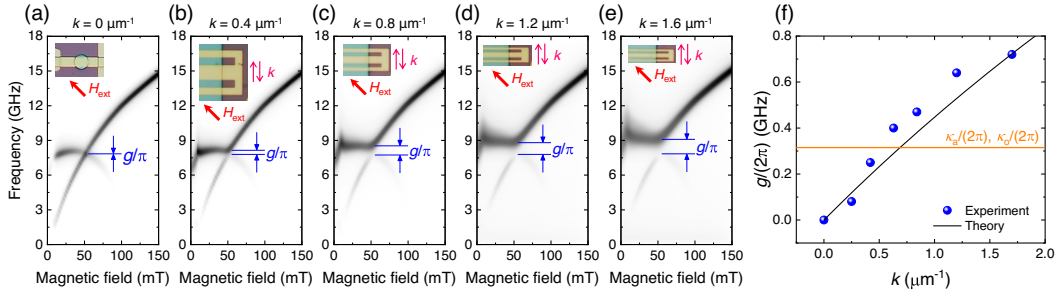

FIG. 3. Contour plots of $\mathrm{Re}[S_{11}]$ spectra at $\varphi_k = 45°$ with (a) $k = 0$, (b) 0.4, (c) 0.8, (d) 1.2, and (e) 1.6 $\mu\mathrm{m}^{-1}$. (f) $g/(2\pi)$ as a function of k. The orange solid line indicates the dissipation rates of both the resonance modes κ_a and κ_o, determined from the half width of half maximum linewidth in the FMR spectra.

coupled via interlayer exchange coupling, where the energy per unit area is denoted as J_{ex}. In addition, dynamic dipolar interaction appears in the presence of spin waves due to the nonuniform distribution of local magnetic moments. Therefore, the effective magnetic field $\mathbf{H}_i$ acting on the magnetization $\mathbf{m}_i$ (normalized as $|\mathbf{m}_i| = 1$) of the FMi layer is given by

$$\mathbf{H}_i = H_{\mathrm{ext}}\mathbf{e}_x - M_s m_{zi}\mathbf{e}_z - H_E\mathbf{m}_j + \mathbf{H}_{\mathrm{dip},ii} + \mathbf{H}_{\mathrm{dip},ij} \quad (i, \quad j = 1, 2 \quad \text{and} \quad i \neq j), \tag{1}$$

where the x axis is parallel to the direction of the in-plane magnetic field H_{ext}, whereas the z axis is perpendicular to the sample plane. The second term on the right-hand side of Eq. (1) represents the shape anisotropy (demagnetization) field. The field strength of the interlayer exchange coupling is $H_E = |J_{\mathrm{ex}}|/(M_s t)$, where M_s is the saturation magnetization of the ferromagnet, whereas the last two terms in Eq. (1) correspond to the self- and mutual-dipolar fields [36–38]. In the absence of a spin wave, the magnetizations point in the tilted direction from the external field with an angle $\varphi_0 = \cos^{-1}[H_{\mathrm{ext}}/(2H_E)]$ for $H_{\mathrm{ext}} < 2H_E$. It is convenient for the evaluation of resonance frequencies to introduce $X_iY_iZ_i$ coordinates, where the X_i axis is parallel to the equilibrium direction of uniform magnetization $\mathbf{m}_i$, whereas the Z_i axis is parallel to the z axis. We denote a small-amplitude oscillating component of magnetization around the X_i axis as $\delta\mathbf{m}_i = (0, m_{iY}, m_{iZ})^T$, where the components are defined in the $X_iY_iZ_i$ coordinate, and the superscript T represents the transpose vector. The LL equation can then be linearized by assuming $m_{iX} \simeq 1$ and $|m_{iY}|$, $|m_{iZ}| \ll 1$, and is given by

$$i\omega \begin{pmatrix} m_{1Y} \\ m_{1Z} \\ m_{2Y} \\ m_{2Z} \end{pmatrix} + \mu_0\gamma\hat{\mathbf{H}} \begin{pmatrix} m_{1Y} \\ m_{1Z} \\ m_{2Y} \\ m_{2Z} \end{pmatrix} = 0, \tag{2}$$

where γ is the gyromagnetic ratio. The resonance frequencies $f = \omega/(2\pi)$ are the eigenvalues of the fourth-order matrix $\hat{\mathbf{H}}$. The secular equation for the eigenvalue has the form

$$\omega^4 + a\omega^2 + b\omega + c = 0. \tag{3}$$

The detailed expressions for the matrix $\hat{\mathbf{H}}$ and the coefficients a, b, and c are given in Supplemental Material [35]. First, we evaluate the anticrossing gap from the analytical solutions of Eq. (3) and compare it with the experimental result. The solid lines in Figs. 2(i) and 3(f) represent the theoretical values of the gap as functions of the spin-wave propagation angle and the wave number, respectively, where the values of the parameters are derived from our previous work [30]. Quantitative agreement between the experiment and theory guarantees the validity of the analysis based on the LL equation.

Next, we discuss the origin of the anticrossing gap. The details of the calculations supporting the following discussions are given in Supplemental Material [35]. We note that Eq. (3) is applicable to evaluate the resonant frequencies of FMR by considering the limit of $H_{\mathrm{dip}} \to 0$. Under this condition, the coefficient b in Eq. (3) is zero, because b is proportional to the dipolar field H_{dip}. Then, the solutions of Eq. (3) become $f = \pm f_a, \pm f_o$, where f_a and f_o are the resonant frequencies of the uniform acoustic and optic modes, respectively. The eigenfunctions of these modes can be expressed as $(\delta\mathbf{m}_1, \delta\mathbf{m}_2)^T = (\delta\mathbf{m}_1, \delta\mathbf{m}_1)^T$ and $(\delta\mathbf{m}_1, \delta\mathbf{m}_2)^T = (\delta\mathbf{m}_1, -\delta\mathbf{m}_1)^T$, respectively. The resonant frequencies of the two modes cross at approximately $\varphi_0 = 45°$ under the external magnetic field $H_{\mathrm{ext}} \sim \sqrt{2}H_E$; i.e., the anticrossing gap does not appear. It is also useful to note that the eigenfunctions of FMR have an exchange symmetry of the magnetizations. This symmetry means that the matrix $\hat{\mathbf{H}}$ commutes with an exchange operator $\mathcal{P}$ of the magnetizations, which acts as $\mathcal{P}(\delta\mathbf{m}_1, \delta\mathbf{m}_2)^T = (\delta\mathbf{m}_2, \delta\mathbf{m}_1)^T$. However, in the presence of H_{dip} ($b \neq 0$), the solutions of Eq. (3) are independent of each other, leading to the nonreciprocity of the spin-wave propagation in the SAFs [30,39–42]. The exchange operator $\mathcal{P}$ does not commute with the matrix $\hat{\mathbf{H}}$, indicating that the exchange symmetry of the magnetizations is broken. The resonant frequencies of SWR then have no crossing point; i.e., the anticrossing gap appears. It should be, however, noted that the exchange symmetry of the magnetizations is recovered when the spin wave propagates in the direction parallel to the external magnetic field ($\varphi_k = 0°$). Then, the anticrossing gap disappears. In other words, the appearance of the anticrossing gap accompanies the symmetry breaking with respect to the exchange of the magnetizations. The symmetry breaking occurs due to the asymmetry of the self- and mutual-dipolar fields between two magnetizations, whose magnitudes depend on the relative angle between the magnetizations and spin wave. The asymmetry in these dipolar fields is maximized at approximately $\varphi_k = 45°$. Therefore, the anticrossing gap is also maximized at approximately the same angle, as can be seen in Fig. 2(f).

In summary, we demonstrated a tunable and strong magnon-magnon coupling between acoustic and optic modes in synthetic antiferromagnets. Our Letter demonstrated that the coupling between two modes is mediated by the dipolar fields generated by the magnetization motion of spin waves. Thus, the coupling strength can be controlled by the wave number of excitation spin waves and the angle between the external magnetic field and spin-wave propagation directions. The experimental results quantitatively agree with the theoretical analysis based on the Landau-Lifshitz equation. The theory indicates that the anticrossing gap appears when the exchange symmetry of two

magnetizations is broken due to the excitation of the spin waves. Our findings offer a new approach toward tunable magnon-magnon coupling systems for SAF-based magnonic applications.

We are grateful to S. K. Kim, S. Tamaru, T. Yorozu, and Y. Suzuki for fruitful discussions. This work was partially supported by the JSPS KAKENHI Grants No. JP15H05702, No. 15K21752, No. JP16H05977, No. JP18K19021, No. JP20K15161, No. JP20H00332, and ISHIZUE of Kyoto University Research Development Program.

*shiota-y@scl.kyoto-u.ac.jp
†tomohiro-taniguchi@aist.go.jp

[1] D. Lachance-quirion, Y. Tabuchi, A. Gloppe, K. Usami, and Y. Nakamura, Appl. Phys. Express **12**, 070101 (2019).
[2] H. Huebl, C. W. Zollitsch, J. Lotze, F. Hocke, M. Greifenstein, A. Marx, R. Gross, and S. T. B. Goennenwein, Phys. Rev. Lett. **111**, 127003 (2013).
[3] Y. Tabuchi, S. Ishino, T. Ishikawa, R. Yamazaki, K. Usami, and Y. Nakamura, Phys. Rev. Lett. **113**, 083603 (2014).
[4] M. Goryachev, W. G. Farr, D. L. Creedon, Y. Fan, M. Kostylev, and M. E. Tobar, Phys. Rev. Applied **2**, 054002 (2014).
[5] X. Zhang, C. Zou, L. Jiang, and H. X. Tang, Phys. Rev. Lett. **113**, 156401 (2014).
[6] L. Bai, M. Harder, Y. P. Chen, X. Fan, J. Q. Xiao, and C. M. Hu, Phys. Rev. Lett. **114**, 227201 (2015).
[7] R. Hisatomi, A. Osada, Y. Tabuchi, T. Ishikawa, A. Noguchi, R. Yamazaki, K. Usami, and Y. Nakamura, Phys. Rev. B **93**, 174427 (2016).
[8] A. Osada, R. Hisatomi, A. Noguchi, Y. Tabuchi, R. Yamazaki, K. Usami, M. Sadgrove, R. Yalla, M. Nomura, and Y. Nakamura, Phys. Rev. Lett. **116**, 223601 (2016).
[9] X. Zhang, N. Zhu, C. Zou, and H. X. Tang, Phys. Rev. Lett. **117**, 123605 (2016).
[10] J. A. Haigh, A. Nunnenkamp, A. J. Ramsay, and A. J. Ferguson, Phys. Rev. Lett. **117**, 133602 (2016).
[11] A. F. Kockum, A. Miranowicz, S. De Liberato, S. Savasta, and F. Nori, Nat. Rev. Phys. **1**, 19 (2019).
[12] X. Zhu, S. Saito, A. Kemp, K. Kakuyanagi, S. Karimoto, H. Nakano, W. J. Munro, Y. Tokura, M. S. Everitt, K. Nemoto, M. Kasu, N. Mizuochi, and K. Semba, Nature (London) **478**, 221 (2011).
[13] J. J. Viennot, M. C. Dartiailh, A. Cottet, and T. Kontos, Science **349**, 408 (2015).
[14] Y. Tabuchi, S. Ishino, A. Noguchi, T. Ishikawa, R. Yamazaki, K. Usami, and Y. Nakamura, Science **349**, 405 (2015).
[15] V. V Kruglyak, S. O. Demokritov, and D. Grundler, J. Phys. D **43**, 264001 (2010).
[16] A. A. Serga, A. V. Chumak, and B. Hillebrands, J. Phys. D **43**, 264002 (2010).
[17] A. Khitun, M. Bao, and K. L. Wang, J. Phys. D **43**, 264005 (2010).
[18] A. V. Chumak, V. I. Vasyuchka, A. A. Serga, and B. Hillebrands, Nat. Phys. **11**, 453 (2015).
[19] R. P. Feynman, Found. Phys. **16**, 507 (1986).
[20] T. D. Ladd, F. Jelezko, R. Laflamme, Y. Nakamura, C. Monroe, and J. L. O'Brien, Nature (London) **464**, 45 (2010).
[21] H. J. Kimble, Nature (London) **453**, 1023 (2008).
[22] A. Reiserer and G. Rempe, Rev. Mod. Phys. **87**, 1379 (2015).
[23] C. L. Degen, F. Reinhard, and P. Cappellaro, Rev. Mod. Phys. **89**, 035002 (2017).
[24] S. Klingler, V. Amin, S. Geprägs, K. Ganzhorn, H. Maier-flaig, M. Althammer, H. Huebl, R. Gross, R. D. Mcmichael, M. D. Stiles, S. T. B. Goennenwein, and M. Weiler, Phys. Rev. Lett. **120**, 127201 (2018).
[25] H. Qin, S. J. Hämäläinen, and S. Van Dijken, Sci. Rep. **8**, 5755 (2018).
[26] J. Chen, C. Liu, T. Liu, Y. Xiao, K. Xia, G. E. W. Bauer, M. Wu, and H. Yu, Phys. Rev. Lett. **120**, 217202 (2018).
[27] J. Chen, T. Yu, C. Liu, T. Liu, M. Madami, K. Shen, J. Zhang, S. Tu, M. S. Alam, K. Xia, M. Wu, G. Gubbiotti, Y. M. Blanter, G. E. W. Bauer, and H. Yu, Phys. Rev. B **100**, 104427 (2019).
[28] D. MacNeill, J. T. Hou, D. R. Klein, P. Zhang, P. Jarillo-Herrero, and L. Liu, Phys. Rev. Lett. **123**, 047204 (2019).
[29] L. Liensberger, A. Kamra, H. Maier-flaig, S. Geprägs, A. Erb, S. T. B. Goennenwein, R. Gross, W. Belzig, H. Huebl, and M. Weiler, Phys. Rev. Lett. **123**, 117204 (2019).
[30] M. Ishibashi, Y. Shiota, T. Li, S. Funada, T. Moriyama, and T. Ono, Sci. Adv. **6**, eaaz6931 (2020).
[31] V. Vlaminck and M. Bailleul, Phys. Rev. B **81**, 014425 (2010).
[32] P. Grünberg, R. Schreiber, Y. Pang, M. B. Brodsky, and H. Sowers, Phys. Rev. Lett. **57**, 2442 (1986).
[33] J. J. Krebs, P. Lubitz, A. Chaiken, and G. A. Prinz, Phys. Rev. Lett. **63**, 1645 (1989).
[34] Z. Zhang, L. Zhou, P. E. Wigen, and K. Ounadjela, Phys. Rev. B **50**, 6094 (1994).
[35] See Supplemental Material at http://link.aps.org/supplemental/10.1103/PhysRevLett.125.017203 for a detailed description of the theoretical calculation.
[36] H. Benson and D. L. Mills, Phys. Rev. **178**, 839 (1969).
[37] F. C. Nörtemann, R. L. Stamps, and R. E. Camley, Phys. Rev. B **47**, 11910 (1993).
[38] R. L. Stamps, Phys. Rev. B **49**, 339 (1994).
[39] K. Di, S. X. Feng, S. N. Piramanayagam, V. L. Zhang, H. S. Lim, S. C. Ng, and M. H. Kuok, Sci. Rep. **5**, 10153 (2015).
[40] S. Wintz, V. Tiberkevich, M. Weigand, J. Raabe, J. Lindner, A. Erbe, A. Slavin, and J. Fassbender, Nat. Nanotechnol. **11**, 948 (2016).
[41] V. Sluka, T. Schneider, R. A. Gallardo, A. Kákay, M. Weigand, T. Warnatz, R. Mattheis, A. Roldán-molina, P. Landeros, V. Tiberkevich, A. Slavin, G. Schütz, A. Erbe, A. Deac, J. Lindner, J. Raabe, J. Fassbender, and S. Wintz, Nat. Nanotechnol. **14**, 328 (2019).
[42] R. A. Gallardo, T. Schneider, A. K. Chaurasiya, A. Oelschlägel, S. S. P. K. Arekapudi, R. Hübner, K. Lenz, A. Barman, J. Fassbender, J. Lindner, O. Hellwig, and P. Landeros, Phys. Rev. Applied **12**, 034012 (2019).